Acta Biomaterialia 26 (2015) 295–305

Contents lists available at ScienceDirect

Acta Biomaterialia

journal homepage: www.elsevier.com/locate/actabiomat

Photodynamic therapy of melanoma skin cancer using carbon dot – chlorin e6 – hyaluronate conjugate

Songeun Beack [a], Won Ho Kong [a], Ho Sang Jung [a], In Hwan Do [a], Seulgi Han [a], Hyemin Kim [a], Ki Su Kim [b], Seok Hyun Yun [b], Sei Kwang Hahn [a,*]

[a] Department of Materials Science and Engineering, Pohang University of Science and Technology (POSTECH), 77 Cheongam-ro, Nam-gu, Pohang 790-784, Republic of Korea
[b] Wellman Center for Photomedicine, Massachusetts General Hospital and Harvard Medical School, 65 Landsdowne St., Cambridge, MA 02139, USA

ARTICLE INFO

Article history:
Received 22 May 2015
Received in revised form 15 August 2015
Accepted 19 August 2015
Available online 20 August 2015

Keywords:
Carbon dot
Chlorin e6
Hyaluronate
Transdermal delivery
Photodynamic therapy

ABSTRACT

Despite wide application of photodynamic therapy (PDT) for the treatment of melanoma skin cancers, there are strong biomedical unmet needs for the effective generation of singlet oxygen after targeted delivery of photosensitizers. Here, we investigated a facile PDT of melanoma skin cancer using transdermal carbon dot – chlorine e6 – hyaluronate (Cdot-Ce6-HA) conjugates. The Cdot-Ce6-HA conjugate was synthesized by the coupling reaction of diaminohexane modified HA (DAH-HA) with the carboxylic group of Ce6. The singlet oxygen generation of Cdot-Ce6-HA conjugates in aqueous solution was more significant than that of free Ce6. The enhanced transdermal and intracellular delivery of Cdot-Ce6-HA conjugates to B16F10 melanoma cells in tumor model mice were corroborated by confocal microscopy and two-photon microscopy. The laser irradiation after topical treatment with Cdot-Ce6-HA conjugates resulted in complete suppression of melanoma skin cancers. The antitumor effect was confirmed by histological analysis with H&E staining and TUNEL assay for tumor apoptosis. Taken together, we could confirm the feasibility of Cdot-Ce6-HA conjugate for transdermal PDT of melanoma skin cancers.

Statement of Significance

To our knowledge, this is the first report on a facile transdermal photodynamic therapy (PDT) of melanoma skin cancer using carbon dot – chlorine e6 – hyaluronate (Cdot-Ce6-HA) conjugates.
We found that the singlet oxygen generation of Cdot-Ce6-HA conjugates in aqueous solution was more significant than that of free Ce6.
Confocal microscopy and two-photon microscopy clearly confirmed the enhanced transdermal and intracellular delivery of Cdot-Ce6-HA conjugates to B16F10 melanoma cells in tumor model mice.
Taken together, we could confirm the feasibility of Cdot-Ce6-HA conjugate for transdermal PDT of melanoma skin cancers.

1. Introduction

Photodynamic therapy (PDT) is a promising therapeutic modality for metastatic melanoma skin cancers [1–3]. Three main requisites for an effective PDT include a photosensitizer (PS) delivered to tumor tissues, light with an appropriate wavelength, and oxygen in the tumor site [4,5]. PS activated by light can transfer the photon energy to surrounding oxygen molecules, generating singlet oxygen ($^1O_2$) for the necrosis and/or apoptosis of cancer cells [6]. However, it is known to be difficult to transdermally deliver PS to cancerous tissues due to the limited penetration-depth [7]. Accordingly, target-specific transdermal delivery of PS is strongly needed for effective PDT, preventing normal cells from destruction. Meanwhile, Ce6 as a PS has several advantages for PDT, such as a high singlet oxygen quantum yield of *ca.* 0.75, bright fluorescence at wavelengths of 660–670 nm, and rapid clearance from the body [8]. The drawbacks of Ce6 are its poor water solubility and pharmacokinetics, and lack of tumor targeting. Huang et al. [9] reported a PDT using chlorin e6 (Ce6) conjugated to carbon dot (Cdot). They used Cdot to improve water solubility of Ce6 and extend half-life of Ce6 in blood. In addition, Cdot excited Ce6 indirectly by Förster fluorescence resonance energy transfer (FRET). Cdot has advantages of excitation dependent emission, non-cytotoxicity compared to quantum dots, and cheap synthetic process [9–13].

* Corresponding author.
E-mail address: skhanb@postech.ac.kr (S.K. Hahn).

http://dx.doi.org/10.1016/j.actbio.2015.08.027
1742-7061/

A naturally occurring linear polysaccharide of hyaluronate (HA) has been widely investigated for various drug delivery and tissue engineering applications [14,15]. HA has been also used as a promising transdermal delivery carrier [16–18]. Although the transdermal delivery mechanism of HA is not quite clear yet, hygroscopic HA can hydrate stratum corneum, enhancing the permeability of HA with a hydrophobic patch domain through the skin. Especially, cancerous skin has over-expressed HA receptors such as cluster determinant 44 (CD44) and lymphatic vessel endothelial HA receptor-1 (LYVE-1) on the cellular surface [19]. We have previously reported the HA receptor-mediated transdermal delivery of human growth hormone (hGH) – HA conjugate and nanographene oxide (NGO) – HA conjugate [16,17]. After transdermal delivery, the bioavailability of hGH was as high as 15% [16]. Furthermore, NGO-HA conjugate could be successfully exploited for transdermal photo-ablation therapy of melanoma skin cancer [17].

Here, we report a facile PDT of melanoma skin cancer using transdermal Cdot-Ce6-HA conjugates in the presence of laser irradiation at 660 nm. Melanoma skin cancer is one of the most aggressive and lethal skin cancers. Melanoma is known to grow rapidly into the skin and metastasize [20]. Although PDT has been applied for the treatment of melanoma [21,22], to our knowledge, this is the first report to transdermally deliver Cdot-Ce6-HA conjugate for the treatment of melanoma skin cancers. Tumor tissues over-express HA receptors and have relatively leaky structures. The transdermal delivery of Cdot-Ce6 using HA can be safer and more effective than the systemic delivery, because it is locally accumulated in cancerous skin, making facile repeated administration possible and minimizing the side effect in the body. After *ex vivo* confocal and *in vivo* two-photon fluorescence imaging for the transdermal delivery of Cdot-Ce6-HA conjugates, we assessed and discussed the PDT of Cdot-Ce6-HA conjugates for the treatment of melanoma skin cancer in mice.

2. Materials and methods

2.1. Materials

Sodium hyaluronate (HA) with a molecular weight (MW) of 230 kDa was purchased from Lifecore Co. (Chaska, MN). 1,6-Diaminohexane (DAH) and 3-(4,5-dimethyl-2-thiazolyl)-2,5-diphenyl-2H-tetrazolium bromide (MTT) were obtained from Sigma–Aldrich (St. Louis, MO). Chlorin e6 (Ce6) was purchased from Santa Cruz Biotechnology (Santa Cruz, CA). 1-Ethyl-3-(3-dimethylaminopropyl)carbodiimide (EDC) hydrochloride was purchased from Tokyo Chemical Industry (Tokyo, Japan) and N-hydroxysulfosuccinimide sodium salt (sulfo-NHS) was from Alfa Aesar (Ward Hill, MA). Singlet oxygen sensor green (SOSG) was obtained from Molecular Probe (Eugene, OR). Dulbecco's modified Eagle's medium (DMEM), fetal bovine serum (FBS), antibiotics, and phosphate buffered saline (PBS) were purchased from Invitrogen (Carlsbad, CA). B16F10 murine melanoma was obtained from Korean Cell Line Bank (Seoul, Korea). Calcein-AM and propidium iodide (PI) were supplied from AnaSpec (Fremont, CA). The eight chamber glass slides with polystyrene vessels were purchased from BD Falcon (Franklin Lakes, NJ). DeadEnd Fluorometric TUNEL system was obtained from Promega (Madison, WI).

2.2. Preparation of Cdot-Ce6-HA conjugate

Carbon dot (Cdot), Ce6 conjugated Cdot (Cdot-Ce6), and diaminohexane modified HA (DAH-HA) were synthesized as reported elsewhere [9,23,24]. Cdot was synthesized by the thermal decomposition of glycerin [23]. In brief, 15 mL of glycerin and 1 g of PEG-$(NH_2)_2$ were mixed for 10 min degassing with nitrogen. After the temperature increased to 270 °C, the degassing solution was quickly mixed with 1 g of citric acid, reacted at the temperature for 3 h, and then cooled down to room temperature. The resulting black solution was dialyzed against deionized (DI) water using a cellulose ester dialysis membrane bag (MWCO = 3500) for 3 days. Cdot-Ce6 was synthesized using EDC/NHS chemistry [9]. Ce6 was dissolved in DMSO at a concentration of 1 mg/mL. The carboxyl group of Ce6 was activated with equimolar EDC and NHS for 30 min. Cdot dissolved in PBS at a concentration of 1 mg/mL and the Ce6 solution were mixed at a volume ratio of 2:1 at room temperature for 12 h. After that, Cdot-Ce6 conjugate solution was dialyzed (MWCO = 3000) against DI water for 3 days, PBS for 1 day, ethanol for 1 day, and DI water for 1 day to remove unreacted Ce6 and DMSO. DAH-HA conjugate was also prepared by EDC/NHS chemistry [24]. HA was dissolved in DI water at a concentration of 5 mg/mL. DAH was added to the HA solution (molar ratio of DAH to HA repeating unit = 20). The pH of the reaction mixture was dropped to pH 5.5 by adding 1 N HCl solution, and EDC and sulfo-NHS were added to the reacted solution. The pH of the reaction mixture was maintained at pH 4.8, and stirred for 2 h. After the reaction was stopped by changing the pH to 7.4, the solution was dialyzed (MWCO = 10,000) against 100 mM NaCl solution for 4 days, 25% ethanol solution for 12 h, and DI water for 12 h. DAH-HA conjugate was analyzed by ^{1}H NMR. Finally, Cdot-Ce6 was dissolved in DI water at a concentration of 5 mg/mL. The carboxyl group of Ce6 was activated with equimolar EDC and sulfo-NHS for 30 min. DAH-HA dissolved in DI water at a concentration of 40 mg/mL and activated Cdot-Ce6 solution were mixed at a weight ratio of 4:1 at room temperature. After reaction for 12 h, Cdot-Ce6-HA conjugate solution was dialyzed (MWCO = 10,000) against PBS (pH 7.4, 10 mM) and DI water to remove unreacted Cdot-Ce6 and byproducts.

2.3. Characterization of Cdot-Ce6-HA conjugate

Photo-images of PBS, Ce6, Cdot-Ce6, Cdot-Ce6-HA conjugate solutions were taken with a Galaxy S3 camera (Samsung, Seoul, Korea). UV/Vis spectra and photoluminescent spectroscopy were obtained using a UV spectrophotometer (JASCO J-715, Easton, MD) and a photoluminescence spectrometer (FP-6500, JASCO, Easton, MD). The size and morphology of Cdot-Ce6-HA conjugates were visualized by atomic force microscopy (AFM, VEECO Instrument, New York, NY) and transmission electron microscopy (TEM, Hitachi 7600, Hitachi, Japan) at an operating voltage of 80 kV. The formation of Cdot-Ce6-HA conjugate was confirmed by Fourier transform – infrared spectroscopy (FT-IR, Nicolet 6700 FT-IR spectrometer, Thermo Fisher Scientific, Waltham, MA). The contents of Ce6 in Cdot-Ce6 and Cdot-Ce6-HA conjugates were determined by measuring the absorbance of Ce6 at 650 nm.

2.4. Detection of singlet oxygen

To assess the generation of singlet oxygen, SOSG at a concentration of 2.5 μM was mixed with Ce6, Cdot-Ce6, and Cdot-Ce6-HA conjugates (1 μM of Ce6). Each solution was added to 1 mL quartz cuvette, which was irradiated with a 660 nm portable laser for the specified time. The absorbance of SOSG was measured at 256, 402, and 653 nm, and SOSG fluorescence was excited using a laser at 504 nm. The singlet oxygen generation of samples was detected by comparing SOSG fluorescence with the control sample.

2.5. In vitro photodynamic effect

B16F10 cells at a density of 6×10^3 were seeded on 96-well plates. Ce6, Cdot-Ce6 or Cdot-Ce6-HA conjugate was dissolved in

each cell media at a concentration of 1 μM and incubated for 4 h. Then, cells were washed with fresh media twice. A portable 660 nm laser with a power density of 100 mW/cm^2 was irradiated on each well for 10 min at the same distance to provide the same laser power. After incubation for 24 h, the phototoxicity of each sample was assessed by the standard MTT assay. MTT assay is a colorimetric assay for testing the cellular metabolic activity. MTT is reduced to insoluble purple formazan in living cells. Cells treated in dark were used as a control group. To evaluate the efficacy of PDT, B16F10 cells at a density of 9×10^3 were seeded onto 35 mm culture dishes containing 300 μL of DMEM and incubated for 24 h. Culture medium was replaced with 300 μL of fresh medium containing Ce6, Cdot-Ce6, or Cdot-Ce6-HA conjugates at a dose of 1 μM free Ce6. The dose of Ce6 was determined on the basis of the results reported elsewhere [9,10]. After incubation in dark for 4 h, the cells were replaced with fresh culture medium and irradiated with a 660 nm laser for 10 min. After another incubation for 2 h, the cells were washed with PBS and stained with Calcein-AM and PI.

2.6. Confocal microscopy for cellular uptake

B16F10 cells were incubated at 37 °C and 5% CO_2 in DMEM containing 10 vol% FBS and 1% antibiotics. The cells were seeded on an eight chamber glass slide at a density of 1×10^4 per well and incubated for a day. Then, Ce6, Cdot-Ce6 and Cdot-Ce6-HA conjugates (1 μM of free Ce6 equivalent) in 200 μL of DMEM were added to the wells. To confirm HA receptor-mediated endocytosis of Cdot-Ce6-HA conjugate, the cells were incubated with 100-fold excess of HA for 2 h before Cdot-Ce6-HA conjugate treatment. After 2 h incubation, the cells were washed with PBS twice and fixed with 4% paraformaldehyde solution for 20 min. The nuclei were stained and mounted with Vectashield mounting medium containing 4′,6′-

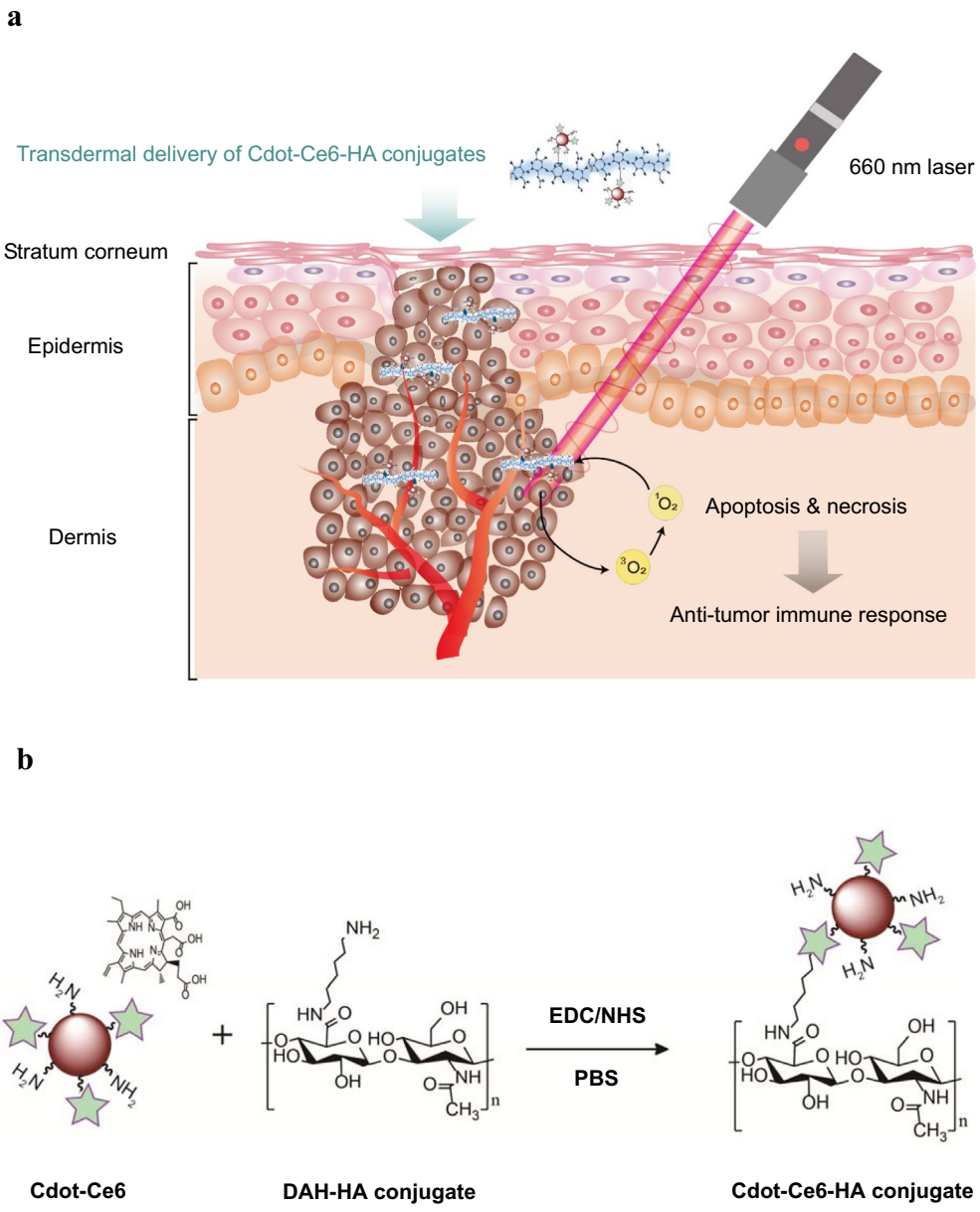

Fig. 1. Schematic illustration for (a) the photodynamic therapy of melanoma skin cancers after transdermal delivery of carbon dot – chlorin e6 – hyaluronate (Cdot-Ce6-HA) conjugate and (b) the synthesis of Cdot-Ce6-HA conjugate using the EDC/NHS chemistry.

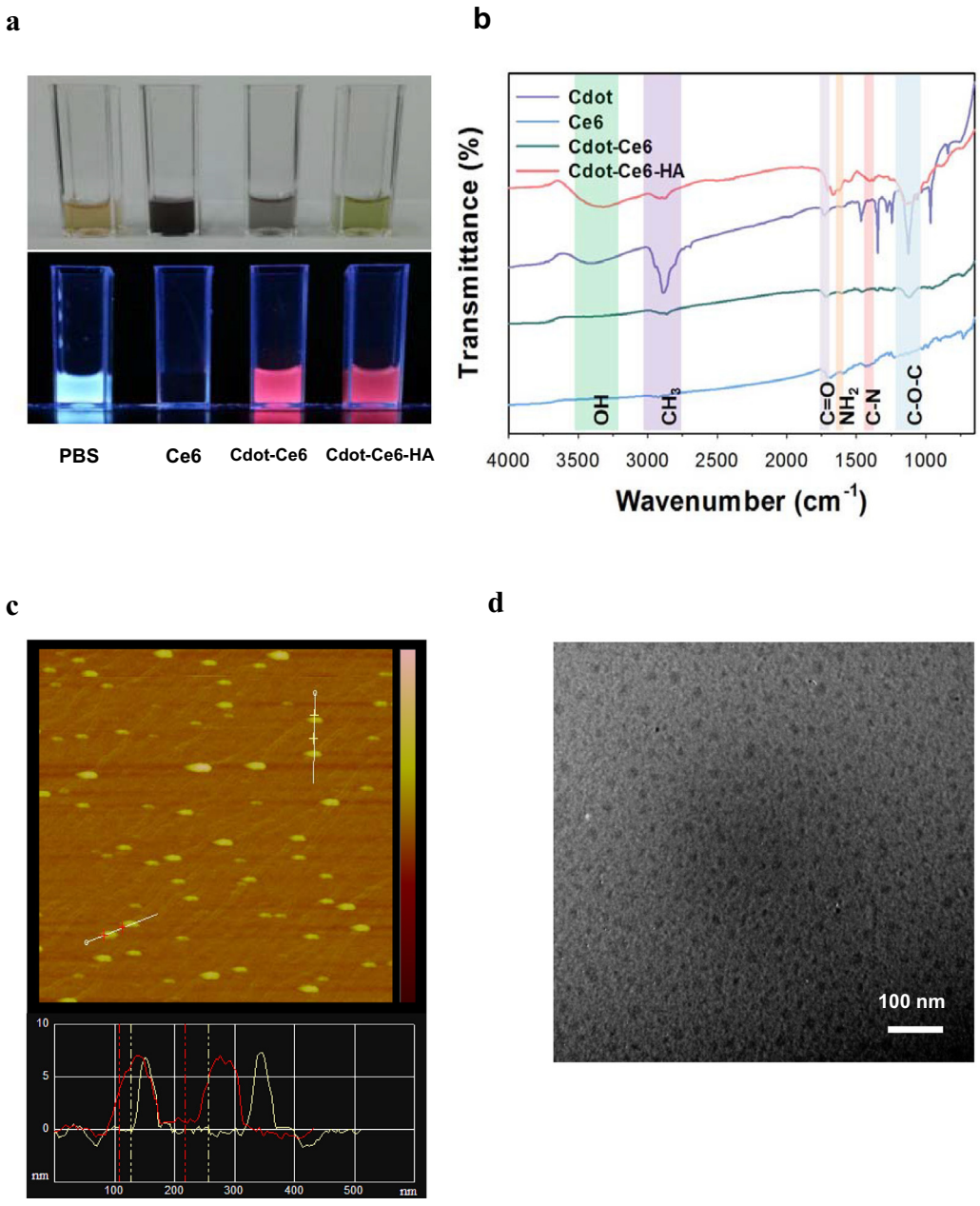

Fig. 2. (a) Photo-images and fluorescence images of Cdot, Ce6, Cdot-Ce6, and Cdot-Ce6-HA conjugate in distilled water. (b) FT-IR analysis of Cdot, Ce6, Cdot-Ce6, and Cdot-Ce6-HA conjugate. (c) AFM and (d) TEM images showing the morphology of Cdot-Ce6-HA conjugates.

diamidino-2-phenylindole (DAPI). The cellular uptake of Cdot-Ce6-HA conjugates was assessed by confocal microscopy.

2.7. Ex vivo and in vivo bioimaging of cancerous skins

Skin cancer model mice were prepared by inoculation of B16F10 cells at a density of 1×10^7 to the dorsal flank of SKH-1 hairless mice. After a week, the tumor volume increased to an average size of 70 mm^3 ($n = 3$, twice). Then, PBS, Ce6, Cdot-Ce6, or Cdot-Ce6-HA conjugate was topically administered on the cancerous skin for 30 min and washed with DI water three times. After topical administration, the fluorescence images of dissected tumors were obtained using IVIS imaging systems at the excitation and emission wavelengths of 630 and 680 nm. The transdermal delivery efficiency of Cdot-Ce6-HA conjugates was compared with those of Cdot-Ce6 and Ce6 by using captured fluorescence intensities at the wavelength of 680 nm. *In vivo* two-photon imaging was carried out with Leica TCS SP5II MP SMD FLIM (Leica, Deerfield, IL). The two-photon fluorescence signal of Cdot-Ce6-HA conjugates and second harmonic generation (SHG) of collagen structure were observed at the wavelength of 900 nm. The images were collected as Z-stacks (*xyz*, 400 Hz) at 512×512 pixels and analyzed with LAS AF Lite 2.6.1 of Leica and Image J. The mice were randomized to the groups and the researchers were blinded to the treatments.

2.8. In vivo photodynamic therapy of skin cancers

To assess therapeutic efficacy of Ce6, Cdot-Ce6, and Cdot-Ce6-HA conjugate, skin cancer model mice were prepared as described above. When the tumor volume increased to an average size of 70 mm^3 in a week ($n = 3$, twice), PBS, Ce6, Cdot-Ce6, or Cdot-Ce6-HA conjugate was topically administered on the cancerous skin

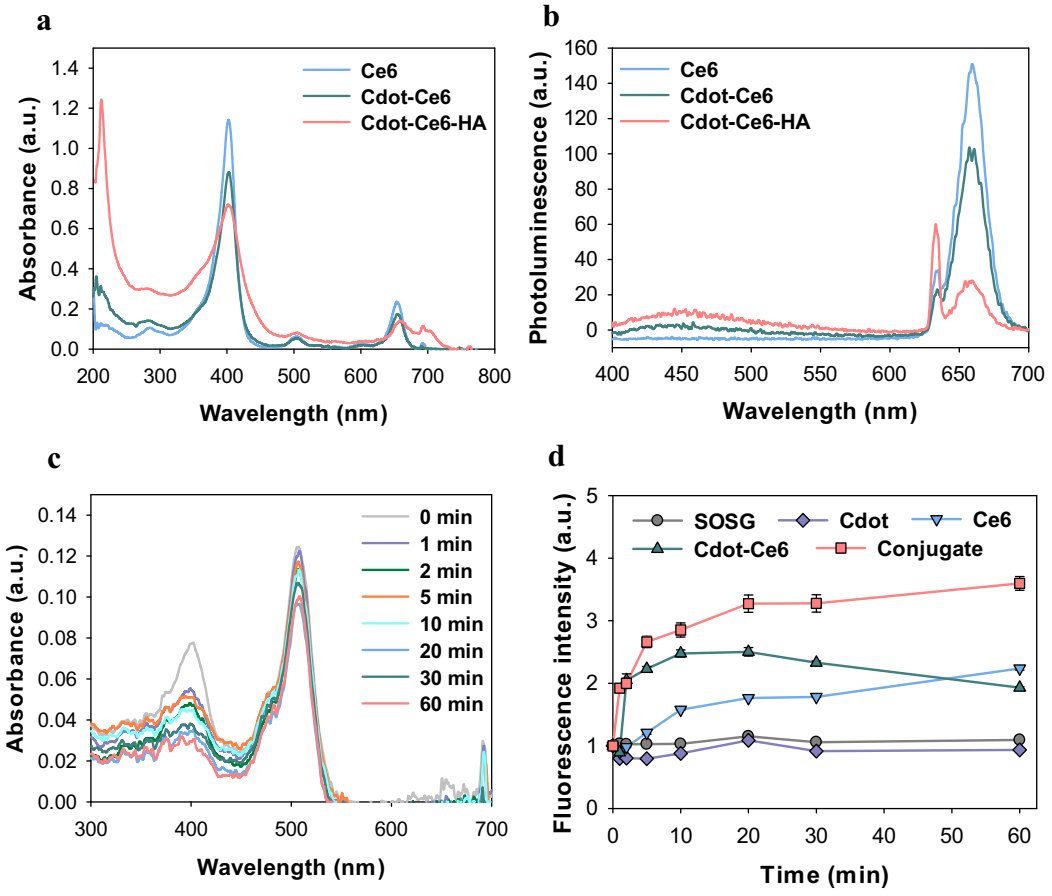

Fig. 3. (a) UV/Vis absorption and (b) photoluminescence emission spectra (ex. 630 nm) of Ce6, Cdot-Ce6, and Cdot-Ce6-HA conjugate in PBS (pH = 7.4). (c) Time-dependent absorbance spectra of singlet oxygen sensor green (SOSG) after generating singlet oxygen with Cdot-Ce6-HA conjugate. (d) The changes of fluorescence emission intensity from SOSG in solutions containing different agents, measured at 530 nm with increasing laser irradiation time. (For interpretation of the references to color in this figure legend, the reader is referred to the web version of this article.)

for 30 min. After washing with DI water thrice, tumors were irradiated with a 660 nm laser for 10 min for the PDT. The tumor growth was monitored by measuring the diameters of tumors with a caliper. The tumor volume was calculated using the following equation: $V = \pi/6 \times A \times B^2$, where A and B are the maximum and minimum diameter of the tumor [25]. We have complied with the POSTECH institutional ethical protocols for animals.

2.9. Histological analysis

To evaluate the anti-cancer efficacy of PDT, tumor tissues were harvested for the histological analysis of tumor apoptosis. PBS was used as a control for the treatment. After topical administration of Ce6, Cdot-Ce6 or Cdot-Ce6-HA conjugate into cancerous skins, the whole tumor tissues were dissected 12 h after the laser treatment and fixed in 4% paraformaldehyde solution. Tumor tissues were made to paraffin-embedded blocks and analyzed by histological analysis with H&E staining and TUNEL assay according to the manufacturer's instruction.

2.10. Statistical analysis

The data are expressed as means ± standard deviation from several separate experiments. Statistical analysis was carried out via the t-test using the software of SigmaPlot 10.0. The values for $^{*}P < 0.05$ and $^{***}P < 0.001$ were considered statistically significant.

3. Results and discussion

3.1. Preparation and characterization of Cdot-Ce6-HA conjugate

As previously reported elsewhere [9], Cdot-Ce6 was prepared by coupling reaction of Ce6 and Cdot in DMSO. Cdot-Ce6-HA conjugate was prepared by amide bond formation between Cdot-Ce6 and DAH-HA in PBS using the EDC chemistry (Fig. 1). Because three carboxyl groups of HA were reported to be the recognition site of HA receptors [26], HA with a DAH content of 10 mol% was prepared to facilitate receptor mediated transdermal delivery of Cdot-Ce6-HA conjugate into skin tissues. Cdot-Ce6-HA conjugates were characterized by microscopy under white light and UV light, FT-IR, AFM, and TEM (Fig. 2). Cdot emits blue fluorescence under UV excitation. Cdot-Ce6-HA conjugate showed higher solubility in aqueous solution than free Ce6 and Cdot-Ce6. Cdot-Ce6-HA conjugate was stable in various biological solutions such as water, 100 mM of NaCl solution, PBS (pH 7.4), serum, and media (Fig. S1a). In contrast, Ce6 was aggregated in water by the hydrophobic interaction, resulting in the fluorescence quenching. Cdot-Ce6 and Cdot-Ce6-HA conjugate showed red fluorescence under UV excitation (Fig. 2a). The FT-IR spectrum of Cdot-Ce6-HA conjugate was similar with that of Cdot-Ce6 (Fig. 2b), which had the characteristic peaks of amide bonds at 1467, 1650, and 1707 cm^{-1}. The peaks at 2900 and 3313 cm^{-1} correspond to the methyl group ($-CH_3$) and the hydroxyl group (–OH) of HA. As shown in AFM images, Cdot had a thickness of *ca.* 2–4 nm

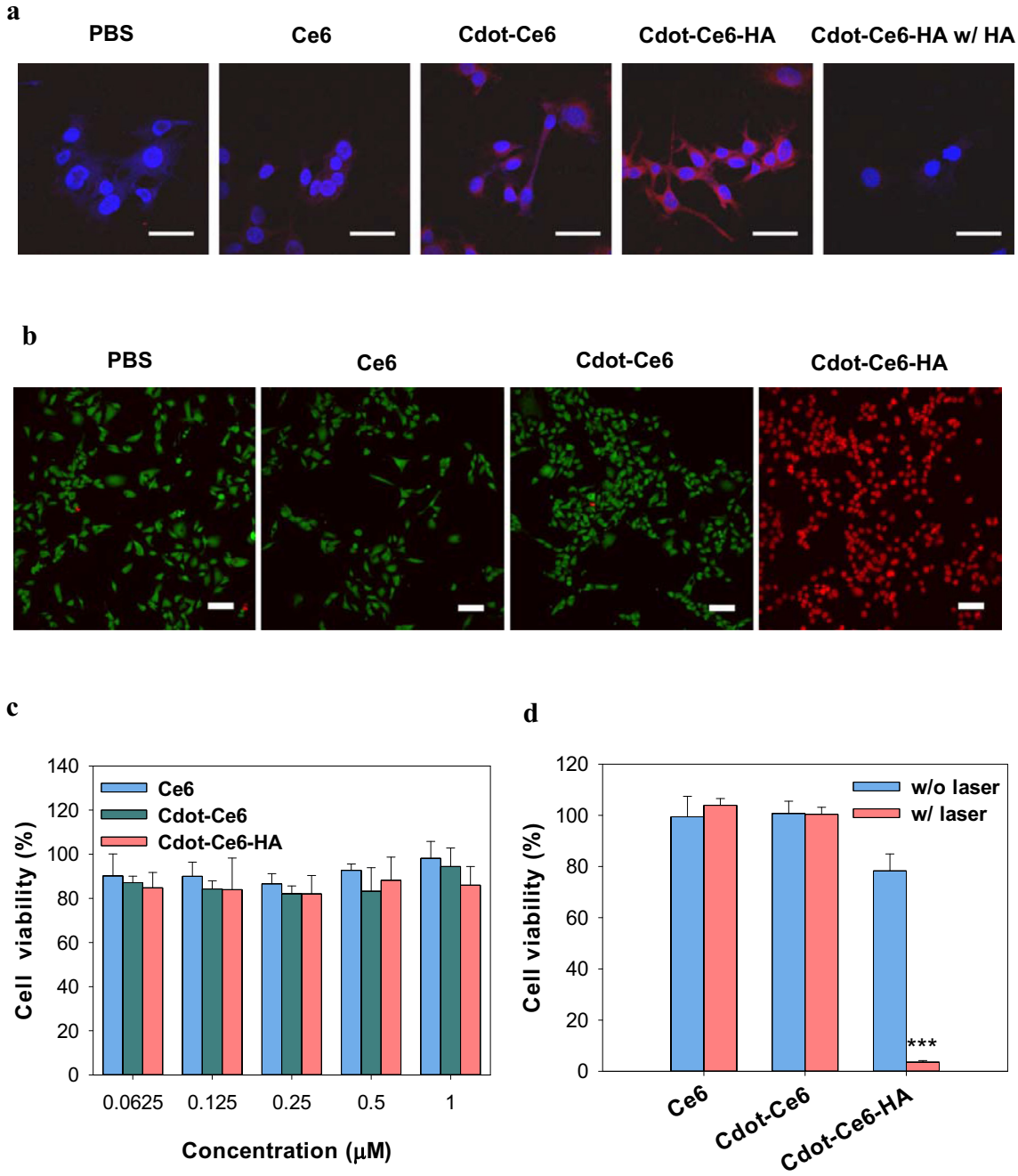

Fig. 4. (a) Confocal microscopy of B16F10 cells after treatment with PBS, Ce6, Cdot-Ce6, or Cdot-Ce6-HA conjugate (scale bars = 50 μm) without and with HA pre-incubation (blue: DAPI, red: Ce6). (b) Live/dead assay after *in vitro* PDT with PBS, Ce6, Cdot-Ce6, or Cdot-Ce6-HA conjugate (scale bars = 100 μm) (green: Calcein AM, red: PI). Cell viability after treatment of B16F10 cells with Ce6, Cdot-Ce6, or Cdot-Ce6-HA conjugate (c) in the absence and (d) presence of laser irradiation for 10 min ($^{***}P < 0.001$, Cdot-Ce6-HA conjugate with laser irradiation *vs* without laser irradiation). (For interpretation of the references to color in this figure legend, the reader is referred to the web version of this article.)

(Fig. S1b) and Cdot-Ce6-HA conjugate had a thickness of *ca.* 6–8 nm (Fig. 2c). TEM revealed a spherical morphology of Cdot-Ce6-HA conjugate with a mean particle size of *ca.* 11–12 nm (Fig. 2d). All of these results confirmed the successful synthesis of Cdot-Ce6-HA conjugate.

3.2. Photochemical properties of Cdot-Ce6-HA conjugate

The photochemical property of Cdot-Ce6-HA conjugates was investigated by optical absorption and photoluminescence spectroscopy. Cdot had no absorbance at 500–800 nm (Fig. S1c). Fig. 3a shows the absorbance spectra of Ce6, Cdot-Ce6, and Cdot-Ce6-HA conjugate in PBS (pH = 7.4). The spectra of Cdot-Ce6 and Cdot-Ce6-HA conjugate were similar with that of Ce6 solubilized in PBS except the high intensity at 200–300 nm and the peak shape at 600–700 nm. These differences might stem from the absorbance of HA at 200–300 nm and interaction between Ce6 and Cdot. Cdot-Ce6-HA conjugate had a micelle structure in PBS due to the hydrophobic domain of Ce6 and the hydrophilic domain of HA. The fluorescence intensity of Cdot-Ce6-HA conjugate was smaller than those of Ce6 and Cdot-Ce6 at the equimolar quantities of Ce6, which was likely due to

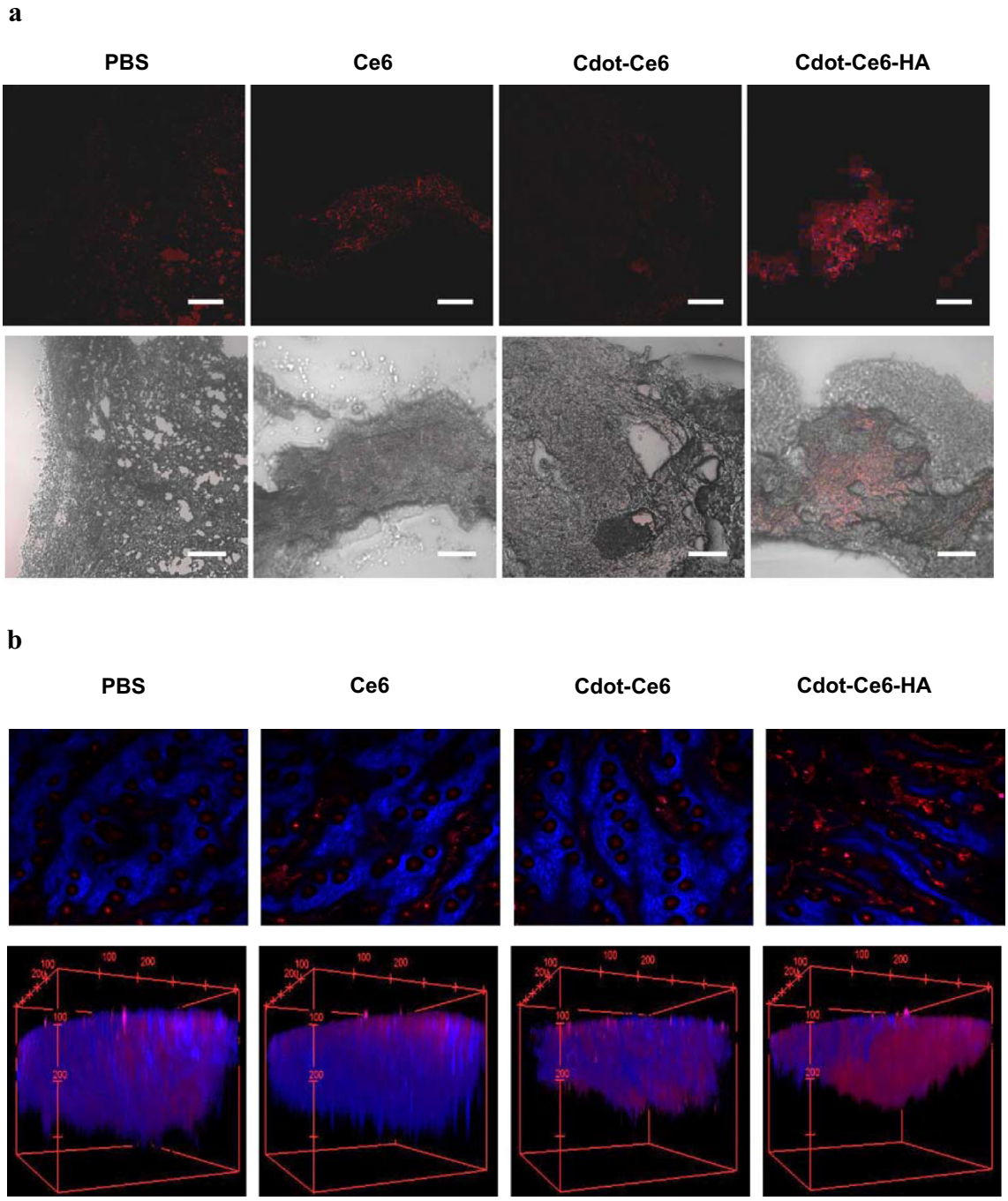

Fig. 5. (a) Confocal (top) and merged (bottom) images of cryo-sectioned cancerous mouse skin tissues after topical treatment with PBS, Ce6, Cdot-Ce6, and Cdot-Ce6-HA conjugates (scale bars = 200 μm). Red fluorescence corresponds to Ce6. (b) Two-photon microscopic cross-sectional views at the Z-stack of 60 μm and 3D two-photon fluorescence images of excised tumors without skin tissues after topical treatment with PBS, Ce6, Cdot-Ce6, and Cdot-Ce6-HA conjugates (blue: collagen, red: Ce6). (For interpretation of the references to color in this figure legend, the reader is referred to the web version of this article.)

self-quenching effect in the micellar structure (Fig. 3b). Furthermore, the emission peak of Cdot-Ce6-HA conjugate was equal to Ce6 irrespective of excitation wavelength (Fig. S1d), whereas the emission wavelength of Cdot was changed depending on the excitation wavelength (Fig. S1e). The absorbance spectrum of Cdot-Ce6-HA conjugate in Fig. 3a was similar to the excitation spectra of Cdot-Ce6-HA conjugate in Fig. S1f. The generation of singlet oxygen from Cdot-Ce6-HA conjugate was confirmed by measuring the changes of absorbance, optical density (OD), and fluorescence signal of SOSG (1 μM) mixed with Cdot-Ce6-HA conjugate (2 μM of Ce6) (Fig. 3c). Endoperoxide generated from SOSG reacted with singlet oxygen emits green fluorescence [27]. The fluorescence intensity of Cdot-Ce6-HA conjugate was higher than that of free Ce6 or Cdot-Ce6 in PBS (Fig. 3d). For the case of SOSG alone or Cdot in the presence of laser irradiation, the fluorescence intensity was not changed, reflecting that Cdot cannot generate singlet oxygen. The photoactivity of free Ce6 in PBS was low likely due to self-quenching by the aggregation with increasing time. In contrast, Cdot-Ce6-HA conjugate without aggregation resulted in significantly higher singlet oxygen generation than Ce6 and Cdot-Ce6 in the presence of laser irradiation (Fig. 3d).

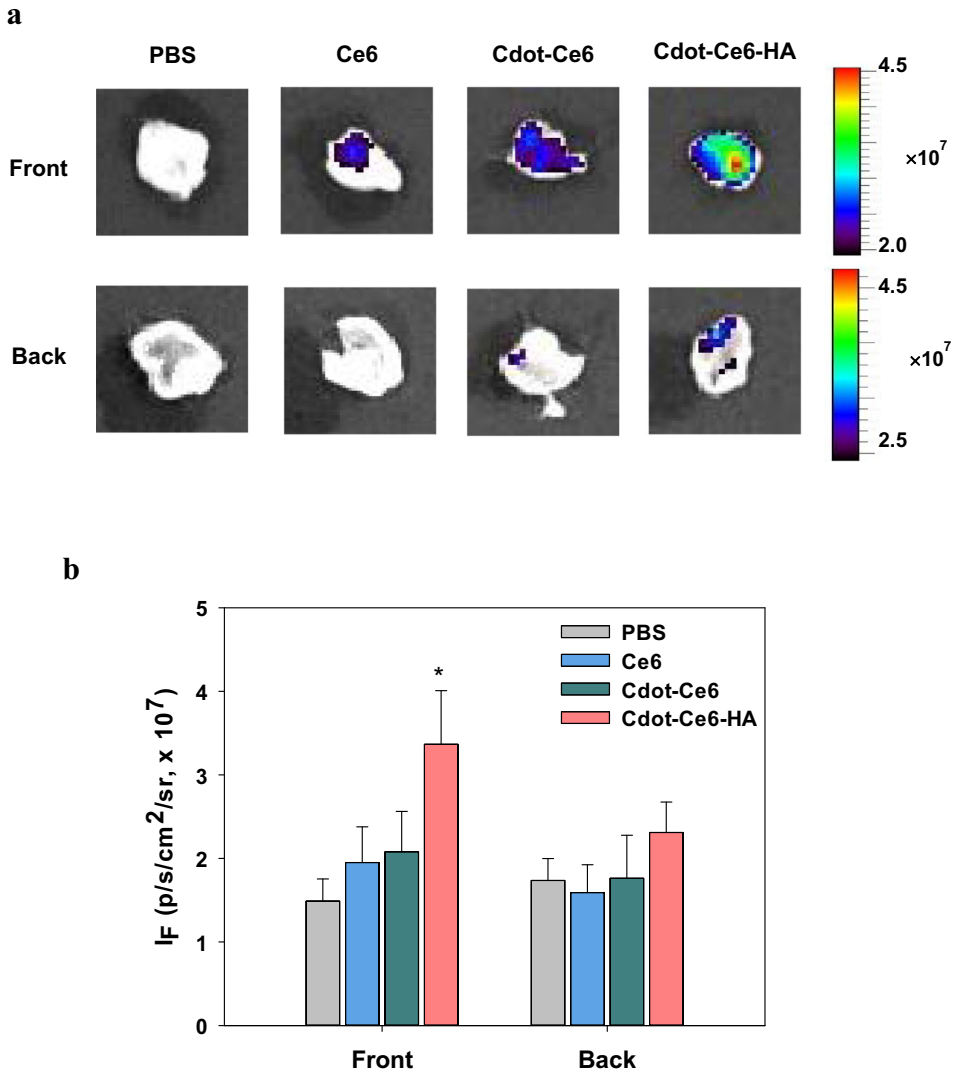

Fig. 6. (a) *Ex vivo* bioimaging of excised tumor tissues (front and back). Color bar represents the red fluorescence intensity. (b) Relative fluorescence intensities from front tissue (in the skin direction) and back tissue ($^{*}P < 0.05$, Cdot-Ce6-HA conjugate *vs* Cdot-Ce6). (For interpretation of the references to color in this figure legend, the reader is referred to the web version of this article.)

3.3. In vitro photodynamic effect of Cdot-Ce6-HA conjugate

Confocal microscopy successfully visualized the effective intracellular delivery of Cdot-Ce6-HA conjugate to B16F10 melanoma cells by HA receptor-mediated endocytosis (Fig. 4a). The red fluorescence of Ce6 was clearly observed in the cell whose nucleus was stained in blue with DAPI. B16F10 cells are known to express HA receptors such as a CD44 and LYVE-1 [28]. The cells pre-incubated with excess HA showed no red fluorescence. Free HA binds to HA receptors on the cell surface, inhibiting the intracellular uptake of Cdot-Ce6-HA conjugates by HA receptor mediated endocytosis. The photodynamic effect of Cdot-Ce6-HA conjugate on B16F10 cells by HA receptor mediated endocytosis was verified by live/dead assay with Calcein AM and PI co-staining (Fig. 4b). In the control group, the majority of cells were alive showing green fluorescence due to negligible photodynamic effect. The treatment with Ce6 and Cdot-Ce6 showed the similar results with the control. In contrast, Cdot-Ce6-HA conjugate resulted in almost complete cell death, exhibiting red fluorescence. According to the MTT assay, the cytotoxicity of Cdot-Ce6-HA conjugate was not significant up to the concentration of 1 μM, but slightly higher than those of Ce6 and Cdot-Ce6 (Fig. 4c). The photodynamic effect of Cdot-Ce6-HA conjugate was analyzed in B16F10 melanoma cells in the absence and presence of 660 nm red laser irradiation (Fig. 4d). Cdot-Ce6-HA conjugate showed much more significant photodynamic effect on cancer cells than Ce6 and Cdot-Ce6, which might be ascribed to the more effective uptake of Cdot-Ce6-HA conjugate to the cells *via* HA-receptor mediated endocytosis.

3.4. Bioimaging for transdermal delivery of Cdot-Ce6-HA conjugate in vivo

The transdermal delivery of Cdot-Ce6-HA conjugate was investigated by confocal microscopy (Figs. 5a and S2a), two-photon microscopy (Figs. 5b and S2b), and fluorescence imaging (Fig. 6). Confocal microscopy showed the red fluorescence of Cdot-Ce6-HA conjugate mainly in cancerous tissues of tumor model mice inoculated with B16F10 cells (Fig. 5a). In contrast, only a small amount of Cdot-Ce6-HA conjugate was delivered through the normal skin (Fig. S2a). Furthermore, two-photon microscopy showed 3D images of skin tissues treated with PBS, Ce6, Cdot-Ce6, and Cdot-Ce6-HA conjugate. Two-photon microscopy is one of the various fluorescence imaging techniques which can be used for skin tissue imaging on the basis of intrinsic emission. Skin has endoge-

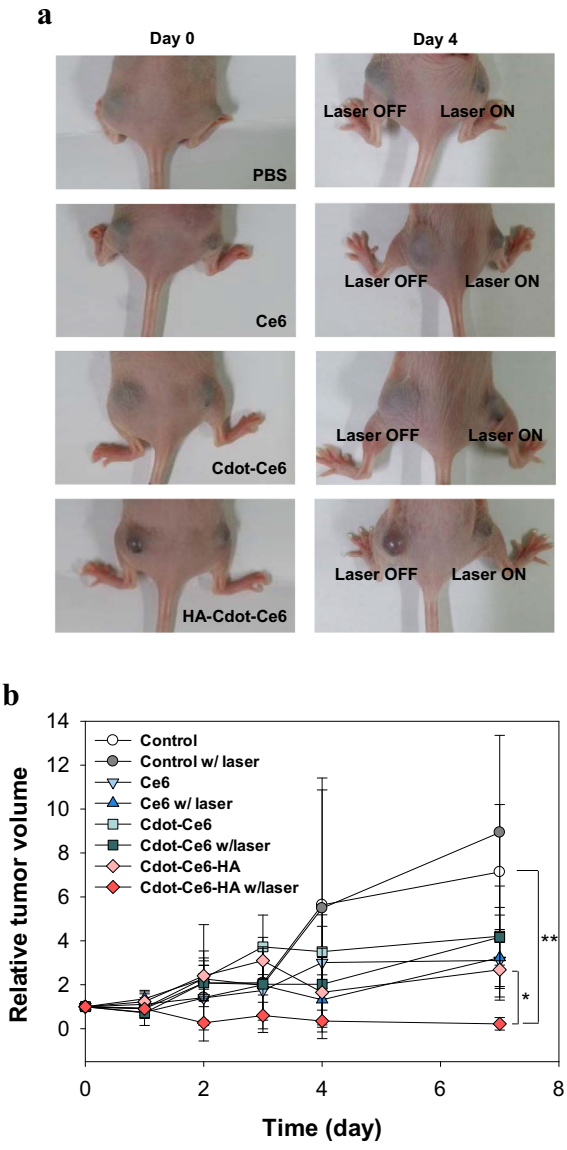

Fig. 7. (a) Photo-images showing the therapeutic effect of photodynamic therapy using PBS, Ce6, Cdot-Ce6, or Cdot-Ce6-HA conjugate in the absence and presence of 660 nm laser irradiation. (b) Relative tumor volume (V/V_0) for up to 7 days after photodynamic therapy ($^{**}P < 0.01$, Cdot-Ce6-HA conjugate *vs* normal control, and $^{*}P < 0.05$, Cdot-Ce6-HA conjugate with laser *vs* without laser).

nous fluorophores such as NAD(P)H, FAD, elastin, and collagen [29], the autofluorescence of which facilitates the study of biological structures in the skin. Collagen shows the SHG signals, which can distinguish dermis from epidermis. Blue colored regions in Fig. 5b represent the dermis composed of collagen, elastin, and proteoglycans. The red fluorescence of Cdot-Ce6-HA conjugate in the tissues was much stronger than those of other samples below dermis where melanoma cancer was inoculated. In contrast, Cdot-Ce6-HA conjugate was mainly observed on top of the normal skin (Fig. S2b).

The fluorescence of Cdot-Ce6-HA conjugate could be detected from the front and back sides of the cancerous skin (Fig. 6a). On the other hand, Ce6 and Cdot-Ce6 were not delivered significantly through the cancerous skin. After topical delivery, the remaining Ce6 and Cdot-Ce6 were removed during the washing step. The quantified signals obtained from IVIS imaging systems revealed that Cdot-Ce6-HA conjugate was more significantly delivered into the deep cancerous skins than the others (Fig. 6b). Normal skin has HA receptors, but tumor tissue is known to express more HA receptors [17]. Taking these results into account, we could confirm the successful transdermal delivery of Cdot-Ce6-HA conjugate to cancerous skin tissues.

3.5. In vivo photodynamic therapy of melanoma skin cancers

SKH-1 hairless tumor model mice with a tumor volume of 70 mm^3 were topically treated with 10 μM of Ce6, Cdot-Ce6, or Cdot-Ce6-HA conjugate using PBS as a control (Fig. 7a). Only one side of the cancerous skin was irradiated with laser, whereas the other side of the skin was not irradiated for comparison. The volume of skin cancer treated with PBS, Ce6, and Cdot-Ce6 increased over time regardless of laser irradiation (Fig. 7b). The difference of tumor volume change even without laser irradiation might be attributed to the activation of Ce6 by sunlight, causing meaningful cytotoxicity in tumor cells [30]. The photosensitivity of Ce6 was reported to be maintained in the skin for 3–7 days [31]. In the case of Cdot-Ce6-HA conjugate, the tumor volume increased without laser irradiation, but significantly suppressed in the presence of laser irradiation by the photodynamic effect.

The anti-tumor effect was assessed by histological analysis of tumor tissues with H&E staining and TUNEL assay 12 h after laser irradiation. As shown in Fig. 8a, cell nuclei stained blue, and intracellular and extracellular proteins stained pink. Pyknosis was observed in tumor tissues after treatment with Cdot-Ce6-HA conjugate in the presence of laser irradiation, reflecting necrosis or apoptosis of tumor cells. Pyknosis is the irreversible condensation of chromatin in the nucleus of a cell, usually associated with necrosis or apoptosis [32]. However, cell death was negligible in tumor tissues treated with PBS, Ce6, and Cdot-Ce6 regardless of laser irradiation. To observe singlet oxygen-induced apoptosis by PDT, the tumor sections treated with PBS, Ce6, Cdot-Ce6, and Cdot-Ce6-HA conjugate in the absence and presence of laser irradiation were analyzed by fluorescence TUNEL assay (Fig. 8b). TUNEL assay is used to detect DNA fragmentation caused by apoptosis [33]. Normal cell nuclei stain blue and TUNEL-positive areas stain green. The tissue sections treated with PBS, Ce6, and Cdot-Ce6 had little green fluorescence in the tumor region. Remarkably, after treatment with Cdot-Ce6-HA conjugate, 660 nm laser irradiation resulted in much more cellular apoptosis than that without laser irradiation, making all the tumor area green. From the results, we could confirm the feasibility of Cdot-Ce6-HA conjugate for target-specific transdermal PDT of melanoma skin cancer.

4. Conclusion

Cdot-Ce6-HA conjugate was synthesized by amide bond formation between amine group of DAH-HA and carboxyl group of Cdot-Ce6 using the EDC chemistry. UV–Vis spectra, PL spectra, FT-IR, AFM, and TEM analyses confirmed the successful synthesis of Cdot-Ce6-HA conjugate. SOSG assay revealed the more effective generation of singlet oxygen by Cdot-Ce6-HA conjugate than Ce6 and Cdot-Ce6 due to enhanced water solubility. According to *in vitro* PDT in B16F10 cells, the photodynamic effect of Cdot-Ce6-HA conjugate was much higher than that of free Ce6 and Cdot-Ce6. Confocal microscopy, two-photon microscopy, and IVIS imaging clearly visualized the effective transdermal delivery of Cdot-Ce6-HA conjugate to cancerous skin tissues. The laser irradiation after treatment with Cdot-Ce6-HA conjugate resulted in statistically more significant suppression of tumor growth than that without laser irradiation. The anti-tumor effect of PDT with Cdot-Ce6-HA conjugate was confirmed by histological analysis with H&E staining and TUNEL assay. Taken together, Cdot-Ce6-HA conjugate might have a great potential for transdermal PDT of melanoma skin cancer.

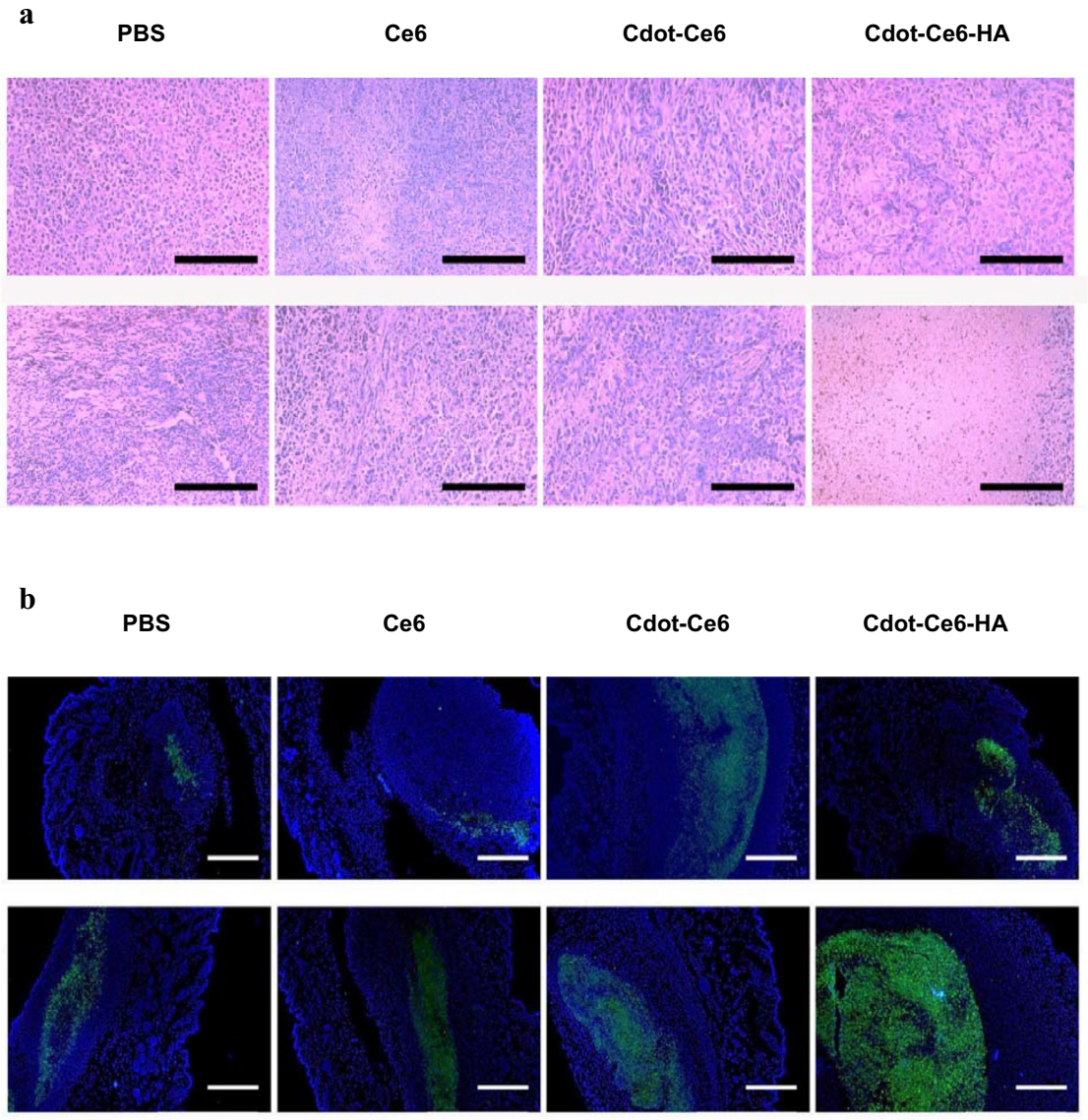

Fig. 8. (a) Histological analysis of cancerous skin tissues with H&E staining after treatment with PBS, Ce6, Cdot-Ce6, or Cdot-Ce6-HA conjugate in the absence (top) and presence (bottom) of laser irradiation (black scale bar = 200 μm). (b) TUNEL assays of cancerous skin tissues after treatment with PBS, Ce6, Cdot-Ce6, and Cdot-Ce6-HA conjugate in the absence (top) and presence (bottom) of laser irradiation (white scale bar = 500 μm, blue: normal cell nuclei, green: TUNEL-positive area). (For interpretation of the references to color in this figure legend, the reader is referred to the web version of this article.)

Acknowledgments

This study was supported by Mid-career Researcher Program through NRF Grant funded by the MEST (No. 2012R1A2A2A06045773). This research was supported by a grant of the Korean Health Technology R&D Project, Ministry of Health and Welfare, Korea (HI14C1658). This research was supported by the MSIP (Ministry of Science, ICT and Future Planning), Korea, under the "IT Consilience Creative Program" (NIPA-2014-H0201-14-1001) supervised by the NIPA (National IT Industry Promotion Agency). We appreciate the technical assistance of Hoe-Yune Jung with the use of the IVIS spectrum facility supported by the Pohang Center for Evaluation of Biomaterials (Pohang Technopark).

Appendix A. Supplementary data

Supplementary data associated with this article can be found, in the online version, at http://dx.doi.org/10.1016/j.actbio.2015.08.027.

References

[1] R. Lincoln, L. Kohler, S. Monro, H. Yin, M. Stephenson, R. Zong, A. Chouai, C. Dorsey, R. Hennigar, R.P. Thummel, S.A. McFarland, Exploitation of long-lived ^{3}IL excited states for metal-organic photodynamic therapy: verification in a metastatic melanoma model, J. Am. Chem. Soc. 135 (2013) 17161–17175.
[2] J. Ge, M. Lan, B. Zhou, W. Liu, L. Guo, H. Wang, Q. Jia, G. Niu, X. Huang, H. Zhou, X. Meng, P. Wang, C.S. Lee, W. Zhang, Z. Han, A graphene quantum dot photodynamic therapy agent with high singlet oxygen generation, Nat. Commun. 5 (2014) 4596.
[3] A. Moiyadi, P. Syed, S. Srivastava, Fluorescence-guided surgery of malignant gliomas based on 5-aminolevulinic acid: paradigm shifts but not a panacea, Nat. Rev. Cancer 14 (2014) 146.
[4] J.P. Celli, B.Q. Spring, I. Rizvi, C.L. Evans, K.S. Samkoe, S. Verma, B.W. Pogue, T. Hasan, Imaging and photodynamic therapy: mechanisms, monitoring, and optimization, Chem. Rev. 110 (2010) 2795–2838.
[5] D. Gao, H. Xu, M.A. Philbert, R. Kopelman, Ultrafine hydrogel nanoparticles: synthetic approach and therapeutic application in living cells, Angew. Chem. Int. Ed. 46 (2007) 2224–2227.
[6] J.F. Lovell, M.W. Chan, Q. Qi, J. Chen, G. Zheng, Porphyrin FRET acceptors for apoptosis induction and monitoring, J. Am. Chem. Soc. 133 (2011) 18580–18582.
[7] M.T. Jarvi, M.J. Niedre, M.S. Patterson, B.C. Wilson, The influence of oxygen depletion and photosensitizer triplet-state dynamics during photodynamic

therapy on accurate singlet oxygen luminescence monitoring and analysis of treatment dose response, Photochem. Photobiol. 87 (2011) 223–234.
[8] A. Juzeniene, Chlorin e6-based photosensitizers for photodynamic therapy and photodiagnosis, Photodiagn. Photodyn. Ther. 6 (2009) 94–96.
[9] P. Huang, J. Lin, X. Wang, Z. Wang, C. Zhang, M. He, K. Wang, F. Chen, Z. Li, G. Shen, D. Cui, X. Chen, Light-triggered theranostics based on photosensitizer-conjugated carbon dots for simultaneous enhanced-fluorescence imaging and photodynamic therapy, Adv. Mater. 24 (2012) 5104–5110.
[10] Y. Cho, Y. Choi, Graphene oxide-photosensitizer conjugate as a redox-responsive theranostic agent, Chem. Commun. 48 (2012) 9912–9914.
[11] S.N. Baker, G.A. Baker, Luminescent carbon nanodots: emergent nanolights, Angew. Chem. Int. Ed. 49 (2010) 6726–6744.
[12] B. Kong, A. Zhu, C. Ding, X. Zhao, B. Li, Y. Tian, Carbon dot-based inorganic–organic nanosystem for two-photon imaging and biosensing of pH variation in living cells and tissues, Adv. Mater. 24 (2012) 5844–5848.
[13] S. Zhu, Q. Meng, L. Wang, J. Zhang, Y. Song, H. Jin, K. Zhang, H. Sun, H. Wang, B. Yang, Highly photoluminescent carbon dots for multicolor patterning, sensors, and bioimaging, Angew. Chem. Int. Ed. 125 (2013) 4045–4049.
[14] K.M. Park, J.A. Yang, H. Jung, J. Yeom, J.S. Park, K.H. Park, A.S. Hoffman, S.K. Hahn, K. Kim, *In situ* supramolecular assembly and modular modification of hyaluronic acid hydrogels for 3D cellular engineering, ACS Nano 6 (2012) 2960–2968.
[15] M. Ma, H. Chen, Y. Chen, K. Zhang, X. Wang, X. Cui, J. Shi, Hyaluronic acid-conjugated mesoporous silica nanoparticles: excellent colloidal dispersity in physiological fluids and targeting efficacy, J. Mater. Chem. 22 (2012) 5615–5621.
[16] J.A. Yang, E.S. Kim, J.H. Kwon, H. Kim, J.H. Shim, S.H. Yun, K.Y. Choi, S.K. Hahn, Transdermal delivery of hyaluronic acid – human growth hormone conjugate, Biomaterials 33 (2012) 5947–5954.
[17] H.S. Jung, W.H. Kong, D.K. Sung, M.Y. Lee, S.E. Beack, D.H. Keum, K.S. Kim, S.H. Yun, S.K. Hahn, Nanographene oxide – hyaluronic acid conjugate for photothermal ablation therapy of skin cancer, ACS Nano 8 (2014) 260–268.
[18] M.B. Brown, S.A. Jones, Hyaluronic acid: a unique topical vehicle for the localized delivery of drugs to the skin, J. Eur. Acad. Dermatol. Venerol. 19 (2005) 308–318.
[19] M. Zoller, CD44: can a cancer-initiating cell profit from an abundantly expressed molecule?, Nat Rev. Cancer 11 (2011) 254–267.
[20] M. Colombino, M. Capone, A. Lissia, A. Cossu, C. Rubino, V.D. Giorgi, D. Massi, E. Fonsatti, S. Staibano, O. Nappi, E. Pagani, M. Casula, A. Manca, M.C. Sini, R. Franco, G. Botti, C. Caraco, N. Mozzillo, P.A. Ascierto, G. Palmieri, BRAF/NRAS mutation frequencies among primary tumors and metastases in patients with melanoma, J. Clin. Oncol. 30 (2012) 2522–2529.
[21] I. Baldea, A.G. Filip, Photodynamic therapy in melanoma – an update, J. Physiol. Pharmacol. 63 (2012) 109–118.
[22] N.M. Idris, M.K. Gnanasammandhan, J. Zhang, P.C. Ho, R. Mahendran, Y. Zhang, *In vivo* photodynamic therapy using upconversion nanoparticles as remote-controlled nanotransducers, Nat. Med. 18 (2012) 1580–1585.
[23] F. Wang, S. Pang, L. Wang, Q. Li, M. Kreiter, C. Liu, One-step synthesis of highly luminescent carbon dots in noncoordinating solvents, Chem. Mater. 22 (2010) 4528–4530.
[24] J. Yeom, S.H. Bhang, B.S. Kim, M.S. Seo, E.J. Hwang, I.H. Cho, J.K. Park, S.K. Hahn, Effect of cross-linking reagents for hyaluronic acid hydrogel dermal filters on tissue augmentation and regeneration, Bioconjug. Chem. 21 (2010) 240–247.
[25] J.D. Hoeck, A. Jandke, S.M. Blake, E. Nye, B.S. Dene, S. Brandner, A. Behrens, Fbw7 controls neural stem cell differentiation and progenitor apoptosis via Notch and c-Jun, Nat. Neurosci. 13 (2010) 1365–1372.
[26] S. Banerji, A.J. Wright, M. Nobel, D.J. Mahoney, I.D. Campbell, A.J. Day, D.G. Jackson, Structures of the CD44-hyaluronan complex provide insight into a fundamental carbohydrate–protein interaction, Nat. Struct. Mol. Biol. 14 (2007) 234–239.
[27] L. Xiao, L. Gu, S.B. Howell, M.J. Sailor, Porous silicon nanoparticle photosensitizers for singlet oxygen and their phototoxicity against cancer cells, ACS Nano 5 (2011) 3651–3659.
[28] N.W. Gale, R. Prevo, J. Espinosa, D.J. Ferquson, M.G. Dominquez, G.D. Yancopoulos, G. Thurston, D.G. Jackson, Normal lymphatic development and function in mice deficient for the lymphatic hyaluronan receptor LYVE-1, Mol. Cell. Biol. 27 (2007) 595–604.
[29] J.A. Palero, H.S. De Bruijin, van der Ploeg, van den Heuvel, H.J.C.M. Sterenborg, H.C. Gerritsen, Spectrally resolved multiphoton imaging of *in vivo* and excised mouse skin tissue, Biophys. J. 93 (2007) 992–1007.
[30] J. Wang, G. Zhu, M. You, E. Song, M.I. Shukoor, K. Zhang, M.B. Altman, Y. Chen, Z. Zhu, C.Z. Huang, W. Tan, Assembly of aptamer switch probes and photosensitizer on gold nanorods for targeted photothermal and photodynamic cancer therapy, ACS Nano 6 (2012) 5070–5077.
[31] J. Wang, M. You, E.G. Zhu, M.I. Shukoor, Z. Chen, Z. Zhao, M.B. Altman, Q. Yuan, Z. Zhu, Y. Chen, C.Z. Huang, Photosensitizer-gold nanorod composite for targeted multimodal therapy, Small 9 (2013) 3678–3684.
[32] K. Wohlan, S. Goy, A. Olling, S. Srivaratharajan, H. Tatge, H. Genth, R. Gerhard, Pyknotic cell death induced by *Clostridium difficile* TcdB: chromatin condensation and nuclear blister are induced independently of the glucosyltransferase activity, Cell. Microbiol. 16 (2014) 1678–1692.
[33] K. Kyrylkova, S. Kyryachenko, M. Leid, C. Kioussi, Detection of apoptosis by TUNEL assay, Odontogenesis 887 (2012) 41–47.